geosciences

MDPI

Article

A Three-Dimensional Geological Structure–Property Coupled Modeling Method and Its Applications

Yanbin Zhou [1], Guangchao Wen [1,2,*], Hongbo Xie [1], Yajie Feng [3] and Xiao Zhou [4]

[1] School of Resources and Environment, Henan Polytechnic University, Jiaozuo 454003, China; 212303010038@home.hpu.edu.cn (Y.Z.); xiehb@hpu.edu.cn (H.X.)
[2] Henan Key Laboratory of Coal Measure Unconventional Resources Accumulation and Exploitation, Henan Polytechnic University, Jiaozuo 454003, China
[3] College of Geoexploration Science and Technology, Jilin University, Changchun 130026, China; yjfeng24@mails.jlu.edu.cn
[4] Shaanxi Provincial Coalfield Geology Group Co., Ltd., Xi'an 710021, China
* Correspondence: wengc@hpu.edu.cn

Abstract

To address the separated organization of structural and attribute information in three-dimensional geological modeling for coal mine production, this study presents a three-dimensional geological structure–property coupled modeling method implemented through an integrated voxel-based workflow. A regular voxel model is used as a unified spatial carrier to organize stratigraphic structures, coal seams, boundaries, reserve parameters, and gas content attributes within the same spatial framework. Structural information is first identified under surface and boundary constraints, and attribute values are then assigned within structurally constrained voxel domains. Using production data from the Hemei No. 3 Mine, the method was applied at both mine and working-face scales to evaluate its implementation, engineering consistency, sensitivity, and uncertainty. The results show that the proposed method can jointly represent the coal seam geometry and gas content distribution and can support spatial query and reserve updating. At the mine scale, the voxel-based reserve estimate for the No. 2-1 coal seam differed from the traditional geological block estimate by 1.67%. At the working-face scale, as an engineering consistency check, the relative difference between the voxel-based estimate and the engineering reference estimate decreased from 31% to 8.4% after additional borehole constraints were incorporated. Additional validation and sensitivity tests yielded quantified errors for gas content and working-face coal-seam geometry estimation. The results further show that reserve estimates are affected by voxel resolution and apparent density assumptions, whereas the spatial distribution of gas content estimates is affected by the tested IDW parameters. Therefore, the proposed method provides a practical application-oriented modeling and updating method under the data conditions of the case study, while broader transferability requires further independent validation and more systematic uncertainty analysis.

Keywords: three-dimensional geological model; structure–property coupled modeling; voxel model; resource reserve estimation; dynamic updating

Check for updates

Academic Editor: Hans-Balder Havenith

Received: 25 April 2026
Revised: 16 July 2026
Accepted: 18 July 2026
Published: 25 July 2026

Copyright: © 2026 by the authors. Licensee MDPI, Basel, Switzerland. This article is an open access article distributed under the terms and conditions of the Creative Commons Attribution (CC BY) license.

1. Introduction

At present, China's coal industry is undergoing profound transformation and restructuring, with its high-quality development explicitly oriented toward the core objectives of safety, efficiency, green development, low-carbon development, and intelligence [1].

Against this backdrop, three-dimensional (3D) geological modeling has become a fundamental technical foundation for supporting safe coal production and refined resource management, thereby facilitating the construction of smart mines. Its essential goal is to promote the transition from traditional two-dimensional geological drawings to three-dimensional digital models, enabling transparent management and control of mine geology [2–4]. As an important foundation for smart mine construction, three-dimensional mine geological models can integrate, visualize, and quantify subsurface geological information, thus providing a unified spatial platform for mineral resource estimation, mining design optimization, and hazard early-warning analysis, and laying the foundation for big-data-driven intelligent decision making [5–7]. Recent studies on digital twins in mining further indicate that the dynamic integration of physical mine entities, geological models, monitoring data, and decision-making processes is becoming an important direction for intelligent mining [6]. In international research, 3D geological modeling is likewise recognized as a core technological approach for achieving subsurface transparency and refined resource management, and it has been widely applied in mineral resource evaluation, engineering geological analysis, and modeling in structurally complex regions [8–10]. However, existing 3D geological models still exhibit notable shortcomings, including limited model accuracy, insufficient integration between structural and attribute information, and difficulties in dynamic updating. These limitations make it challenging to satisfy the practical requirements of safe and efficient coal mining and excavation operations [11].

Three-dimensional geological modeling in coal mines is commonly developed from multi-source data, including exploration, mining, borehole, and geological interpretation data, and is further combined with model computation and visualization analysis to support resource evaluation and production decision making [12,13]. From the perspective of modeling philosophy, existing studies can generally be classified into two categories: explicit modeling and implicit modeling. Explicit modeling directly describes the geometry of geological bodies through geometric objects such as stratigraphic interfaces, fault surfaces, and roadway boundaries, whereas implicit modeling reconstructs geological interfaces and spatial relationships by means of continuous mathematical representations, such as distance fields, potential fields, or interpolation functions. TINs, regular grids, voxels, and tetrahedral meshes more accurately reflect the forms of model representation or discrete support schemes, rather than parallel modeling methods in themselves. Considerable progress has been made in the representation of complex geological bodies, multi-source data integration, and three-dimensional visualization. These advances are reflected not only in the development and application of commercial and open-source geological modeling software and workflows [14–16], but also in a range of methodological developments. For example, under conditions involving complex structural zones, refined internal structures of working faces, and multi-source data constraints, spatial statistical methods have been used for fault identification and structural extraction, thereby providing methodological support for the representation of local fine-scale structures [17]. By integrating DEM, geological maps, cross-sections, geophysical data, and other datasets, relatively refined three-dimensional geological models can be established using block-based modeling methods [18]. Implicit modeling methods based on generalized radial basis function interpolation can integrate multiple potential-field datasets, thereby offering possibilities for complex geological interface reconstruction and multi-attribute integration [19,20]. The use of TIN-GTP to construct geological bodies such as coal mine strata, working faces, faults, and collapse columns can also provide model support for geological transparency in mines [21]. In addition, the application of octree structures to the refinement and reconstruction of unstructured meshes such as tetrahedral grids has improved the efficiency and adaptability of three-dimensional morphological reconstruction in structurally complex areas [22–24]. Moreover,

regular grids and voxel models have attracted extensive attention in resource prediction and risk assessment because of their favorable scalability in multi-attribute representation, spatial analysis, and dynamic updating [25–27]. Overall, existing studies have substantially improved the reconstruction and visualization of three-dimensional geological structures in coal mines, but they still mainly focus on the representation and visualization of geological geometry. For applications that are more critical to coal mine production, such as reserve estimation, gas control, and water hazard prevention, structural models of strata, faults, coal pillars, and goafs, and attribute models of gas content, coal seam thickness, density, and water-bearing properties, are still commonly constructed separately in current modeling practice. Attributes are often attached to structural models through post hoc assignment, surface mapping, local interpolation, multisource-data integration, or machine learning-assisted modeling workflows, lacking continuous associations under a unified spatial constraint framework [28,29]. Although this separation between structural and attribute models can satisfy the requirements of model visualization, it makes it difficult to establish mechanisms for continuous attribute representation and coordinated updating under complex geological structural constraints and has become one of the major bottlenecks restricting the refined application of three-dimensional geological modeling [30,31].

In recent years, various efforts have been made to address the problem of structure–property coupling. For example, in subsurface medium modeling and geophysical interpretation, some studies have attempted to incorporate interface geometry and subsurface heterogeneity into a unified inference framework so as to achieve the joint representation of structural and attribute information [32]. In three-dimensional modeling of Quaternary aquifers, hierarchical modeling strategies have also been adopted to organize stratigraphic interfaces and attribute units, thereby improving the integrated representation of multi-level geological objects [33]. These studies indicate that the coordinated organization of structural and attribute information has become an important development direction in three-dimensional geoscientific modeling and also provides useful references for structure–property coupling in coal mine scenarios. In coal mining and related geoscience fields, researchers have further explored the joint representation of structures and attributes from the perspectives of structurally constrained attribute modeling, geostatistical property simulation, random-field-based stratigraphic characterization, probabilistic geological modeling, and machine learning-assisted 3D reconstruction [34,35]. Hybrid data models that combine the advantages of volumetric and vector models provide a basic framework for multi-field coupling in engineering geological space [36]. Attribute interpolation constrained by extracted stratigraphic boundaries can, to some extent, enable structural models to control attribute models [37]. Some studies have also transformed structural models into attribute models and combined them with interpolation methods to achieve the integration of the two [38,39]. In addition, some researchers have attached attribute information to the surface of structural models through color mapping, thereby realizing joint structure–property representation in specific scenarios [40]. More recently, some studies have begun to attempt joint modeling of structures and attributes based on voxel models or probabilistic modeling methods, for example, by using structurally constrained attribute interpolation or random-field models to achieve the coordinated representation of stratigraphic structures and physical property parameters [41,42]. However, existing studies on coupling still face several limitations. First, multiple models are still often constructed independently and then superimposed within a scene, resulting in loose inter-model relationships and making it difficult to establish unified and stable spatial constraints. Second, current three-dimensional modeling is mostly focused on relatively simple geological structures and lacks integrated characterization of both stratigraphic frameworks and internal fine-scale structures. Third, data from different sources, such as surface bore-

holes, underground gas drainage boreholes, and gas inspection points, differ in accuracy, scale, and semantics. The absence of an effective multi-scale data fusion mechanism reduces the reliability of attribute models under heterogeneous data co-constraints and cross-scale inference, thereby limiting their further application in resource development processes.

To address the problems of separated representation of structural and attribute information and insufficient coordinated updating in coal mine three-dimensional geological modeling, this study investigates a structure–property coupled modeling method within a unified spatial representation framework. Using a regular voxel grid as the common spatial carrier, multi-source geological information is organized through a linear index, and structural objects such as strata, coal seams, faults, and boundaries, together with attribute parameters such as gas content and apparent density, are uniformly mapped onto the same discrete spatial units, thereby enabling the organization and representation of attribute information under structural constraints. For modeling requirements at different scales, the proposed method itself remains unchanged; instead, model adaptation is achieved mainly through differences in voxel grid resolution, constraint data types, and statistical scope. Taking production data from the Hemei No. 3 Coal Mine as an example, applications were carried out at both the mine scale and the working-face scale. At the mine scale, stratigraphic structural models for the mining area were constructed mainly based on surface boreholes, mine boundaries, and related horizon control data, and were coupled with attribute parameters such as gas content and apparent density to evaluate the implementation of the proposed method for large-scale unified structure–property representation. At the working-face scale, a refined coal-seam model was constructed mainly using gas drainage roadway boreholes, working-face boundaries, and related geological constraint data, and was further used for model updating and resource reserve analysis to assess its use for local refined representation and dynamic analysis.

Accordingly, this study presents a three-dimensional geological structure–property coupled modeling method implemented as an application-oriented voxel workflow. In this paper, coupling refers to the co-registration of structural labels, property estimates, reserve parameters, and model update states within a common voxel index, together with structure-constrained property assignment. The contribution does not lie in developing a new interpolation algorithm, because conventional Kriging and IDW are adopted in the case study. Rather, it lies in organizing structural recognition, property estimation, spatial query, reserve calculation, and sequential model updating within one reproducible voxel workflow. The case study evaluates the feasibility and engineering consistency of this workflow under the available data conditions, rather than its general predictive validity.

2. Study Area and Data

2.1. Overview of the Study Area

The Hemei No. 3 Mine is located in the eastern part of Heshan District, Hebi City, Henan Province, approximately 22 km from the urban center of Hebi. The principal mining coal seams in the area are the No. 2-1 coal seam of the Shanxi Formation (Permian) and the No. 1-1 coal seam of the Taiyuan Formation. The mining area lies within the transitional zone between the Taihang fault uplift and the Tangyin fault depression. The geological structure is dominated by normal faults, with well-developed folds, and the overall structural complexity is moderate. The coal-bearing strata mainly belong to the Carboniferous–Permian Taiyuan and Shanxi Formations, among which the No. 2-1 coal seam of the Shanxi Formation and the No. 1-1 coal seam of the Taiyuan Formation are the primary mineable seams. The No. 2-1 coal seam is a stable and thick seam that is mineable throughout the entire mining area, with an average thickness of 7.78 m. The No. 1-1 coal seam is a relatively stable medium-thickness seam that is mineable in most

parts of the area, with an average thickness of 1.76 m. The gas geological conditions in the mining area are complex, and the mine is classified as a coal and gas outburst mine. Long-term mining activities have accumulated abundant geological exploration and production data. With the typical geological characteristics of North China-type coalfields, the study area provides an ideal data foundation and research object for investigating and applying the proposed three-dimensional geological structure–property coupled modeling method. Figure 1 illustrates the location of the Hemei No. 3 Mine.

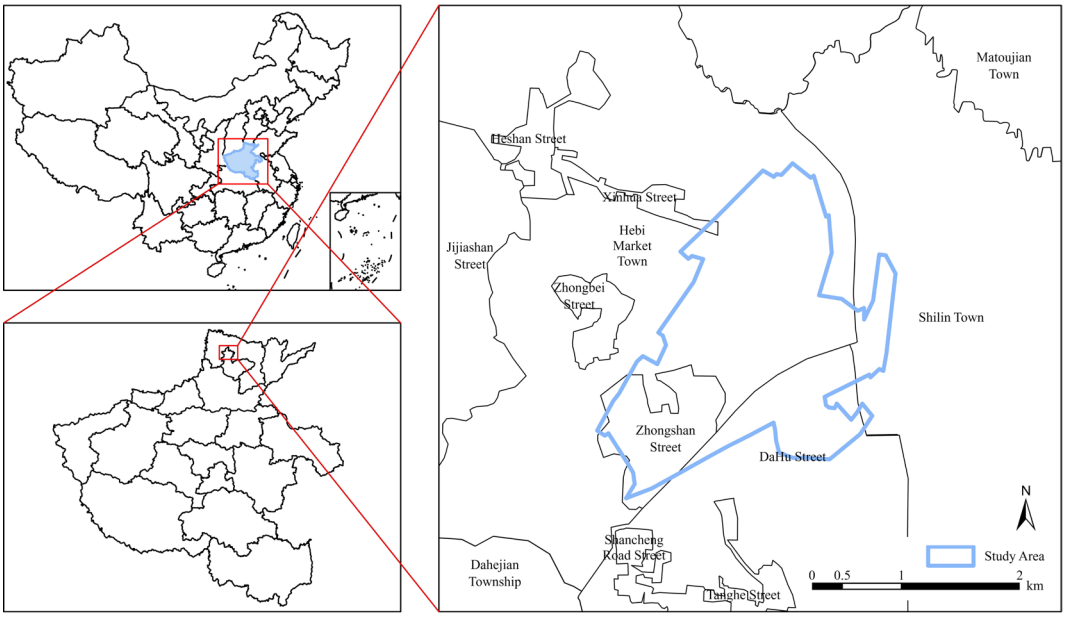


Figure 1. Location map of the study area.

2.2. Data Preprocessing

The data used in this study were derived from the resource reserve verification report, production geological reports, and in situ-measured data of the Hemei No. 3 Mine. Figure 2 illustrates the spatial distribution of surface boreholes, faults, and gas-related data; the symbols are identified in the figure legend. A centralized database was established for unified storage and management of all data. The structural data primarily include 113 surface boreholes and 3403 underground gas drainage roadway boreholes. The attribute dataset contains 555 measured gas content samples. The quantitative geometry validation used 3468 working-face control points; this count refers to modeling control points rather than the number of raw boreholes. After data importation into the database, boundary point coordinates were calculated, as shown in Figures 3 and 4. Owing to the multi-layered stratigraphic characteristics of surface borehole data, multiple boundary points may exist within a single borehole. In contrast, underground gas drainage boreholes retain only the boundary positions of the roof and floor of the coal seam. To ensure the validity of subsequent computations, the data were required to conform to the data structures specified in Tables 1–4 and to satisfy the corresponding constraint conditions. The coordinate system was uniformly adopted as CGCS2000 with a 3° Gauss–Krüger projection zone.

The borehole identification number uniquely identifies each borehole, and the coordinate field records its collar (opening) location. The dip angle ranges from 0° to 90°, and the azimuth ranges from 0° to 360°; the same definitions apply to the underground gas-drainage boreholes. In Table 3, actual depth denotes the total borehole trajectory length and equals the sum of the actual rock depth, actual coal depth, and actual rock penetration depth.

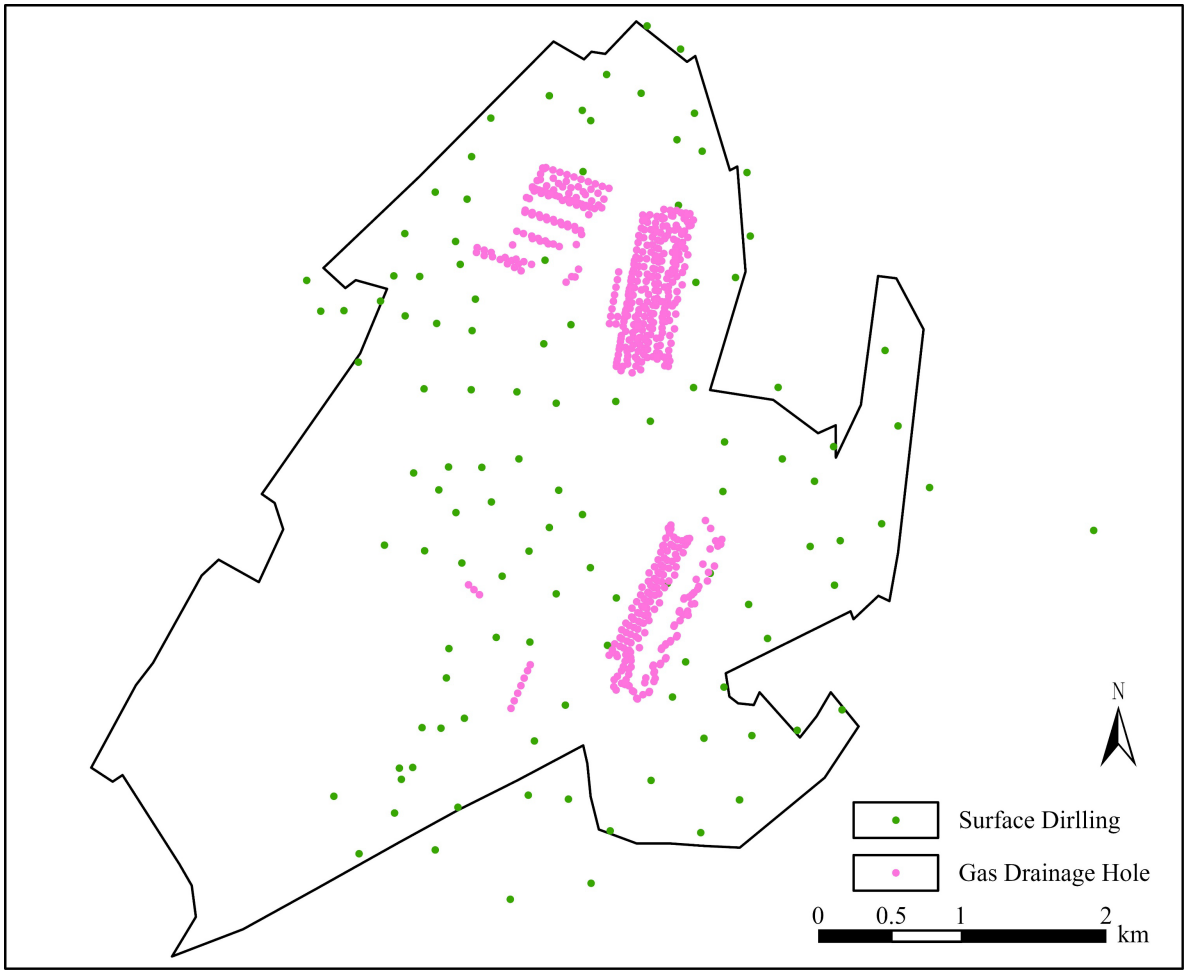


Figure 2. Spatial distribution of the data.

Table 1. Basic information on coal mine boreholes.

Fields	Meaning	Typing	Unit
zkbh	Borehole ID	String	
kkzb	Collar Coordinates	String	
zklx	Borehole Type	String	
ks	Borehole Depth	Float	m
kkrq	Drilling Start Date	String	
zkrq	Drilling End Date	String	
sgdw	Construction Unit	String	
bldw	Logging Unit	String	

Table 2. Borehole lithological information table.

Fields	Meaning	Typing	Unit
zkbh	Borehole ID	String	
cxh	Layer No.	Integer	
ls	Cumulative Depth	Float	m
ch	Layer Thickness	Float	m
qj	Dip Angle	Float	°
fwj	Azimuth	Float	°
yxmc	Lithology Name	String	
yxms	Lithological Description	String	

Table 3. Information table of gas drainage boreholes on the coal mine working face.

Fields	Meaning	Typing	Unit
zkbh	Borehole ID	String	
kkzb	Collar Coordinates	String	
qj	Dip Angle	Float	°
fwj	Azimuth	Float	°
sjsd	Actual Depth	Float	m
sjys	Actual Rock Depth	Float	m
sjms	Actual Coal Depth	Float	m
sjcy	Actual Rock Penetration Depth	Float	m
bz	Remarks	String	

Table 4. Attribute information table (taking gas as an example).

Fields	Meaning	Typing	Unit
bh	Borehole ID	String	
zb	Coordinates	String	
ms	Burial Depth	Float	m
hl	Gas Content	Float	m^3/t
pj	Evaluation	String	

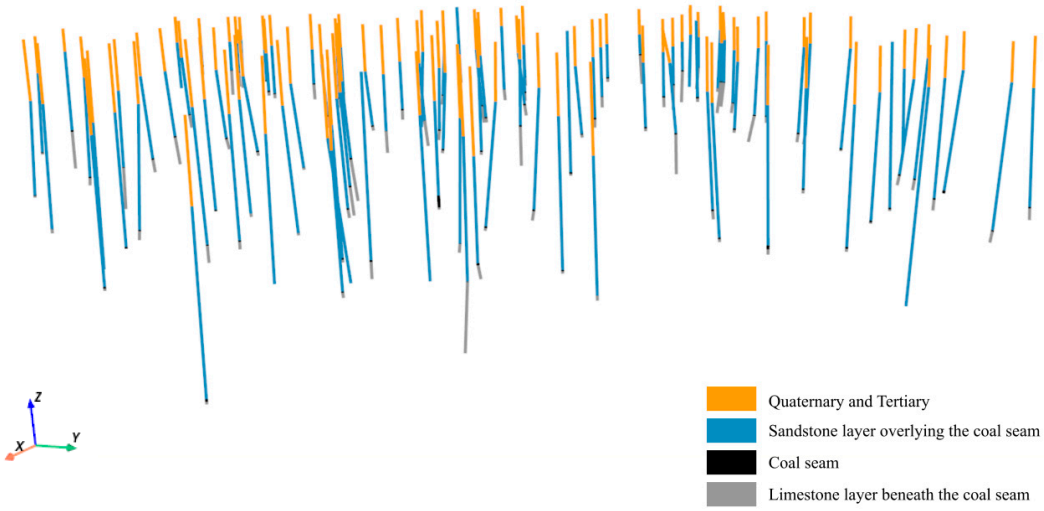


Figure 3. Lithological trajectory of surface boreholes.

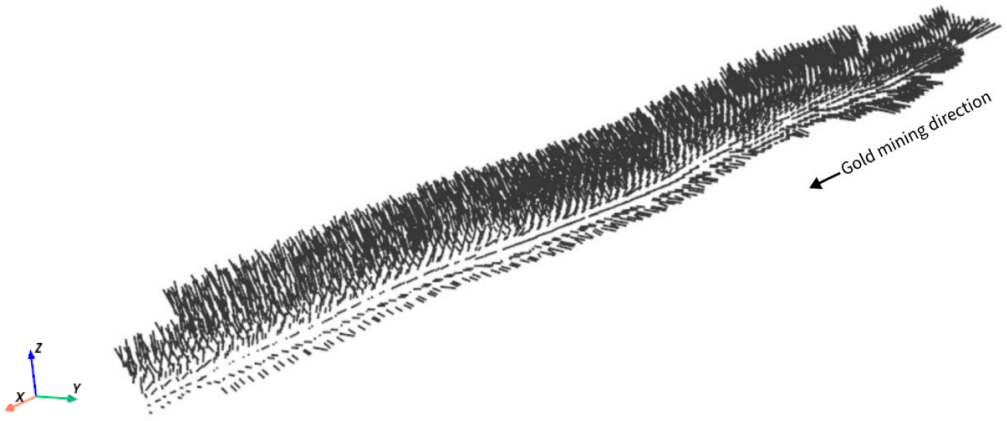


Figure 4. Coal seam trajectory of gas drainage boreholes.

3. Geological Structure–Property Coupled Modeling Method

The proposed workflow comprises five linked operations: (1) define a common voxel domain and resolution; (2) reconstruct continuous geological boundary surfaces from control data; (3) assign a structural label to each voxel by comparing its center with the surfaces and boundary masks; (4) estimate and store property values only in voxels satisfying the required structural label; and (5) aggregate coal seam voxels for reserve calculation and model updating. Structural labels, property values, reserve parameters, spatial indices, and update states are, therefore, co-registered in the same voxel record. When new geological data become available, the affected surfaces and dependent voxel states are reconstructed, after which property assignment and reserve statistics are recalculated. In this operational definition, structure–property coupling denotes common-index organization and structure-constrained property assignment; it does not denote physical process coupling, joint inversion, or a new geostatistical interpolation algorithm. The overall workflow is illustrated in Figure 5.

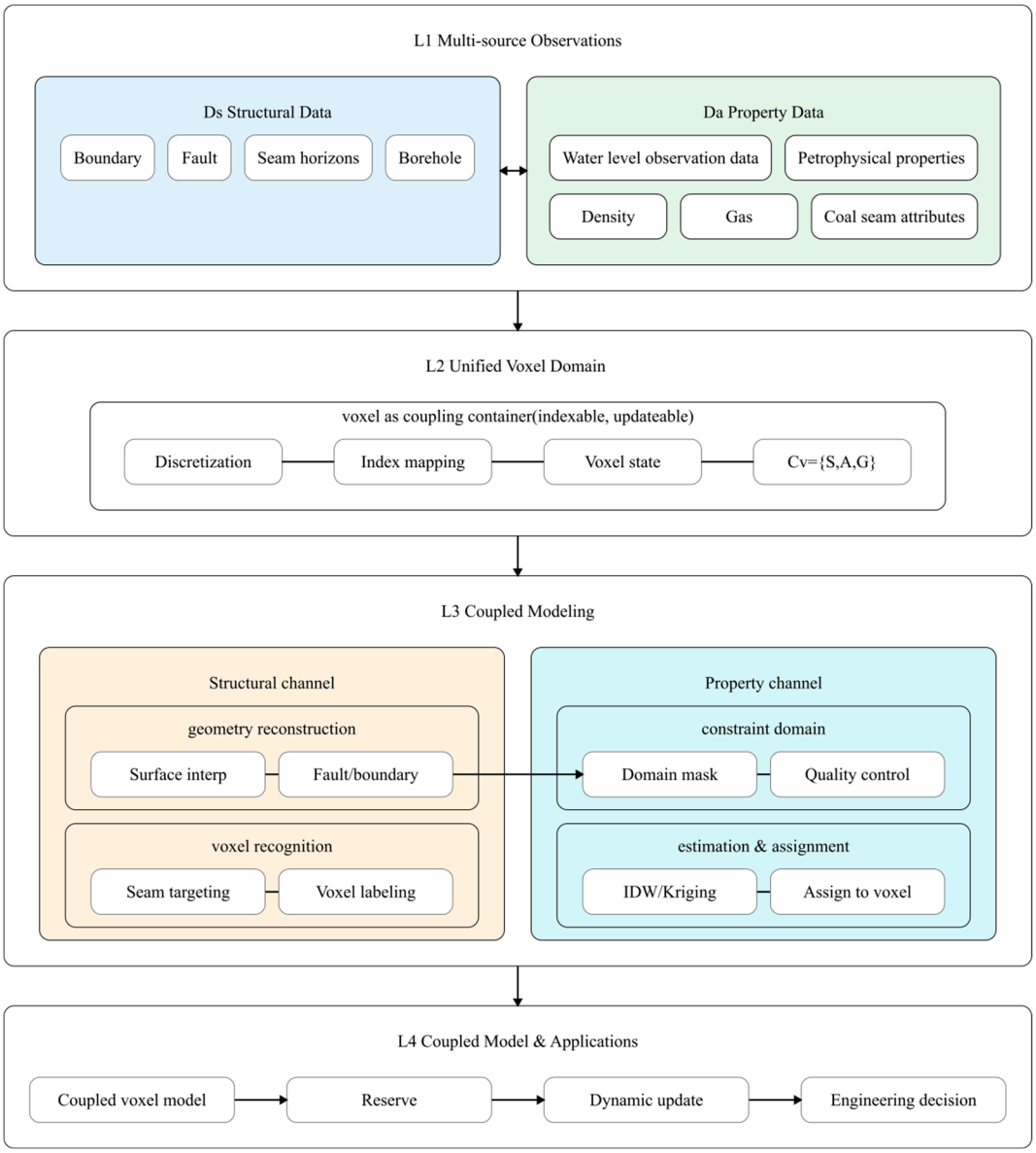


Figure 5. Workflow of the structure–property coupled modeling approach.

3.1. Geological Body Structure Recognition Method

For each coordinate dimension, the modeling domain is bounded by V_{min} and V_{max} and discretized using a specified voxel spacing Δ. Taking V_{min} as the origin, the voxel center coordinates P_i are generated using Equation (1), and the number of voxel centers n is determined using Equation (2). The ceiling operation in Equation (2) allows the regular grid to cover the full coordinate extent; voxels outside the irregular mining boundary are subsequently excluded by a boundary mask. In the two-dimensional example in Figure 6, the blue region is the target domain, the red points are voxel centers inside the domain, and the light-red points are the externally expanded centers retained to guarantee complete coverage before masking.

$$P_i = V_{min} + i\Delta;\ i = 0, 1, 2, \ldots, n-1 \tag{1}$$

$$n = \left\lfloor \frac{V_{max} - V_{min}}{\Delta} \right\rfloor + 1 \tag{2}$$

where P_i denotes the coordinate of the i-th voxel center in the current dimension; V_{min} and V_{max} are the minimum and maximum coordinates, respectively; Δ is the voxel spacing; n is the number of voxel centers along that dimension; and i is a zero-based index ranging from 0 to $n - 1$.

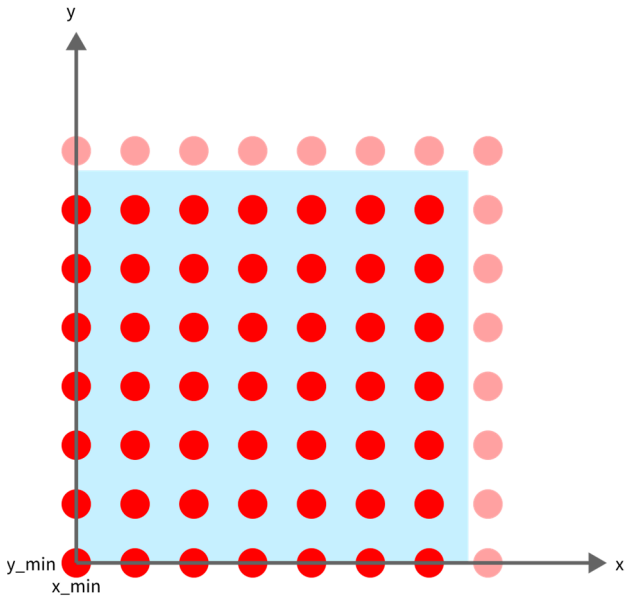


Figure 6. Generation rule of the two-dimensional grid.

After the voxel grid is initialized, each voxel is assigned a zero-based three-dimensional index $I = (I_x, I_y, I_z)$. Equation (3) maps this three-dimensional index to a unique linear index, which is used for voxel lookup, property updating, and regional statistical aggregation.

$$idx = I_x \cdot N_y \cdot N_z + I_y \cdot N_z + I_z \tag{3}$$

where idx is the unique linear index; I_x, I_y, and I_z are the zero-based column, row, and layer indices; and N_x, N_y, and N_z are the numbers of voxels in the corresponding dimensions. The valid index ranges are $0 \leq I_x < N_x$, $0 \leq I_y < N_y$, and $0 \leq I_z < N_z$. The physical center coordinate is recovered from the domain origin and the corresponding index and voxel spacing in each dimension.

The aforementioned method constructs the voxel grid solely from the perspective of spatial discretization and is, therefore, insufficient to fully represent the intrinsic relation-

ship between geological structures and attribute information. Accordingly, it is necessary to introduce a joint structure–property representation mechanism within a unified discretized spatial domain. To prevent voxels from functioning merely as geometric discretization units, this study further defines each voxel as a fundamental state unit for structure–property coupling. For any voxel center point p, its coupled state can be expressed by Equation (4).

$$C_v(p) = \{S(p),\ A(p), G(p)\} \tag{4}$$

where $S(p)$ denotes the structural state, $A(p)$ denotes the property (attribute) state, and $G(p)$ denotes the geometric and auxiliary information. All subsequent modeling and updating processes are carried out based on this voxel unit. On this basis, the structural state of each voxel must first be determined by constructing a continuous structural field and completing voxel-based structural identification, thereby providing spatial constraint conditions for subsequent attribute estimation.

Stratigraphic labeling is performed in four steps. First, continuous boundary surfaces are interpolated from the stratigraphic control points. Second, the surfaces are ordered vertically as $Z_0 > Z_1 > \ldots > Z_n$. Third, the mining-boundary mask is applied to the voxel centers. Finally, Equation (5) compares the elevation P_z of each retained voxel center with the ordered surfaces and assigns either a stratigraphic label L_k or the null label L_{null}.

$$L_P \begin{cases} L_{null} & P_z > Z_0 \text{ or } P_z < Z_n \\ L_k & Z_{k+1} < P_z < Z_k \ k = 0, 1, 2, \ldots, n-1 \end{cases} \tag{5}$$

where Z_0 is the ground-surface elevation, Z_n is the lowest modeled boundary, n is the number of stratigraphic units, and L_k is the label of unit k. The half-open interval $Z_{k+1} < P_z \leq Z_k$ prevents a voxel center on a shared interface from receiving two labels; centers above Z_0 or at or below Z_n receive L_{null}.

The working-face coal-seam model follows the same labeling logic. Roof and floor surfaces are reconstructed from underground gas drainage boreholes, and both the mine boundary and the working-face design boundary are applied as masks. A voxel is labeled as coal only when its center lies inside both masks and between the interpolated roof and floor surfaces.

3.2. Structure–Property Coupling Method

In this study, structural information serves as the prerequisite spatial discriminant condition for attribute information. Therefore, the coupling of attribute information is typically performed under the constraint and guidance of structural information, based on existing attribute data and through interpolation or related computational methods for data fusion. By means of a three-dimensional spatial indexing mechanism, the structural information corresponding to each voxel is retrieved, and attribute values are computed only within structures that satisfy the specified conditions. Before performing the coupling, it is necessary to determine whether a given voxel $v_{m,n,p} = (x_m, y_n, z_p)$ belongs to the specified structural unit v_l, as expressed in Equation (6).

$$\text{value} = \begin{cases} f_A(x_m, y_n, z_p) & v_{m,n,p} \in v_l \\ \text{null} & v_{m,n,p} \notin v_l \end{cases} \tag{6}$$

where $f_A(x_m, y_n, z_p)$ represents the value of the attribute interpolation function (e.g., Kriging, inverse distance weighting, etc.) at voxel $v_{m,n,p}$.

The same assignment logic can be used for continuous or discrete attributes. In this case study, gas content is interpolated only within coal-seam voxels, coal thickness is

derived from the reconstructed roof and floor geometry, and apparent density is stored as the reserve calculation parameter. When a structural surface or voxel label changes, the dependent attribute values and reserve statistics are recalculated for the affected domain.

Interpolation methods were selected according to modeling scale and data density. At the mine scale, ordinary Kriging with a spherical variogram and 20 lags was used to reconstruct regional stratigraphic and coal-seam boundary surfaces; anisotropy was not considered. At the working-face scale, two-dimensional IDW with power = 2, 12 neighbors, and Euclidean distance was used for roof and floor reconstruction. Three-dimensional gas-content interpolation used IDW with power = 2, 15 neighbors, and Euclidean distance within the coal-seam mask. These parameters are summarized in Table 5.

Table 5. Interpolation parameters used in the case study.

Parameter	Value
Kriging Type	Ordinary Kriging
Variogram Model	Spherical
Number of Lags	20
Anisotropy	Not considered
IDW Power	2
IDW Neighbor Number (2D)	12
IDW Neighbor Number (3D)	15
Distance Metric	Euclidean

3.3. Resource Reserve Estimation Method Based on the Coupled Model

Traditional resource reserve estimation is typically carried out by dividing block units on two-dimensional planar maps and calculating reserves using Equation (7).

$$Q = (S/\cos(\alpha)) \cdot M \cdot d \tag{7}$$

where Q denotes the resource quantity of the block, S denotes the horizontal area of the block, M denotes the average coal seam thickness, d denotes the apparent density of the coal seam, and α denotes the dip angle of the coal seam floor.

The resource reserve estimation method based on the coupled model improves upon the traditional block method by replacing the coal seam volume calculation in the block method with volume computation derived from the three-dimensional voxel model. Accordingly, for each voxel belonging to the coal seam, the coal resource quantity can be calculated using Equation (8).

$$Q_j = \sum_{i=1}^{n} V_i \times d \tag{8}$$

where Q_j denotes the resource quantity of the j-th block, V_i denotes the volume of the i-th voxel within the block, d denotes the apparent density of the current coal seam, and n denotes the number of voxels within the current block.

Working-face reserve aggregation: According to the mining design, the target working face (e.g., Working Face 4103) is delineated within the three-dimensional model. All coal seam voxels within this defined range are then selected, and the resource quantities of these voxels are summed to obtain the total resource reserves of the working face. Essentially, this method transforms reserve estimation into a statistical summation of voxel attributes within a specified spatial region, providing a convenient basis for automated reserve statistics.

4. Results

4.1. Integrated Representation of Structure and Properties

Based on surface borehole data, stratigraphic interfaces were constructed using interpolation methods, supplemented by virtual strata to impose constraints from adjacent upper and lower layers and to complete missing stratigraphic information in boreholes. Subsequently, interpolation techniques were applied to generate the stratigraphic surface models, as shown in Figure 7. Under the constraints of the stratigraphic interfaces, a three-dimensional geological structural model of the Hemei No. 3 Mine was constructed using the geological body recognition method (Figure 8). To achieve mine-scale modeling, a voxel resolution of 10 m × 10 m × 4 m was adopted. This resolution was selected according to the modeling scale, data density, and computational requirements, resulting in the construction of approximately 7.0×10^7 voxel units. The model represents the spatial distribution of surface unconsolidated deposits, coal seams, and the overlying and underlying sandstone strata within the mining area, together with their modeled stratigraphic relationships.

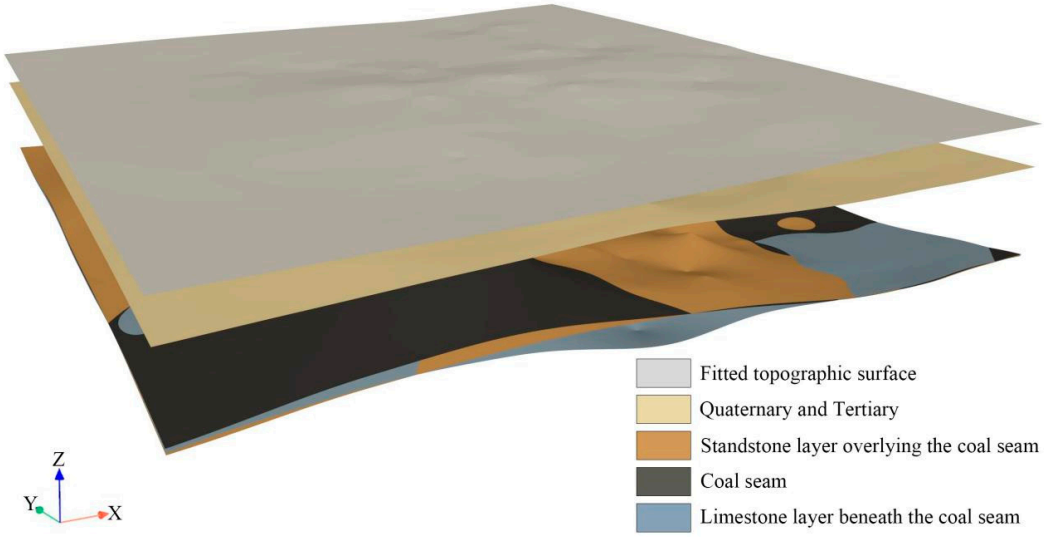


Figure 7. Visualization results of the stratigraphic surfaces.

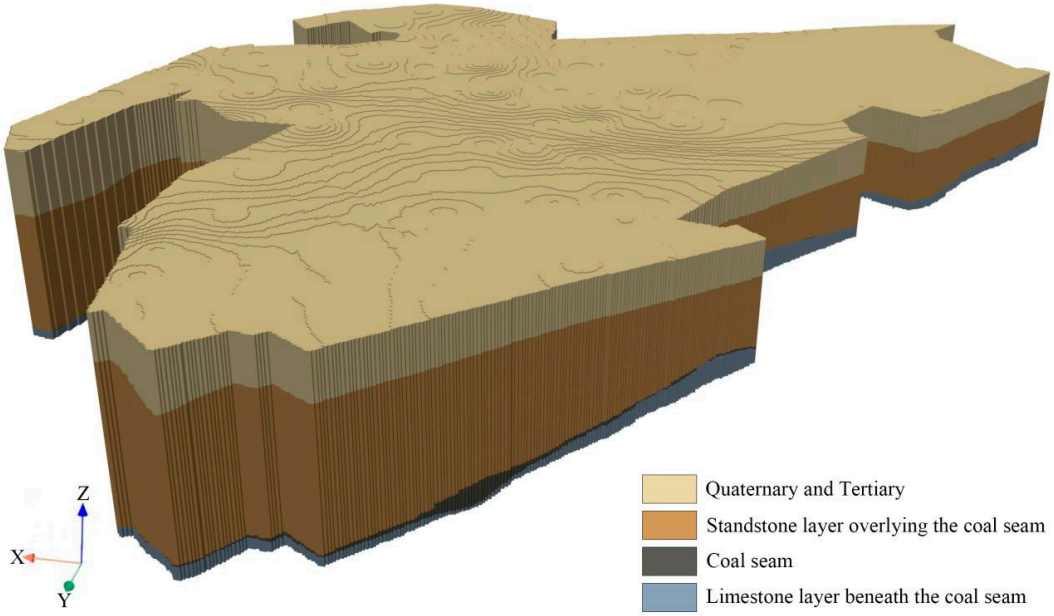


Figure 8. Three-dimensional visualization of the geological structural model.

Based on the above structural model, gas content attributes were coupled to construct the mine-scale structure–property coupled model shown in Figure 9. The model clearly illustrates the variation trends of coal seam thickness along both strike and dip directions, as well as the spatial distribution of gas within the No. 2-1 coal seam, thereby achieving an integrated representation of the structural characteristics and gas properties of the seam. The gas content measurements used for interpolation ranged from 3.94 to 7.68 m^3/t. The blue regions represent areas with relatively lower gas contents, while the purple regions indicate areas with relatively higher gas contents.

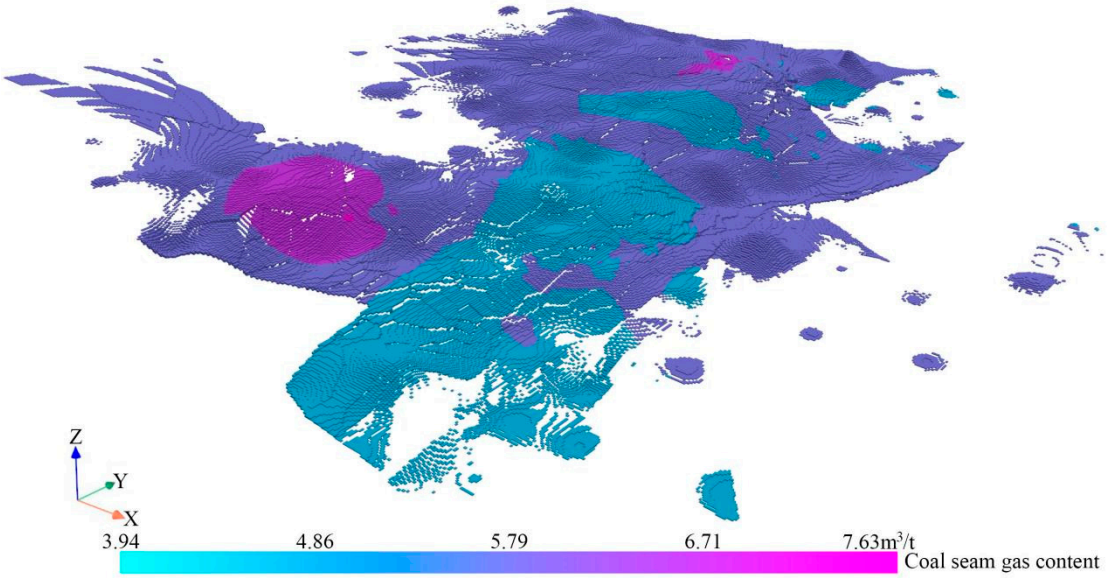


Figure 9. Results of the coupled modeling of geological structure and gas properties.

4.2. Dynamic Estimation of Coal Seam Resource Reserves

Coal seam resource reserve estimation can be categorized into static and dynamic approaches. Static estimation refers to constructing a coal seam model and calculating its reserves based on a given set of exploration data. Dynamic resource estimation, in contrast, reflects the variation in coal seam reserves during the drilling process, as the coal seam model is continuously updated and progressively refined with newly acquired exploration data. Based on the structure–property coupled model, this study employs the voxel-based reserve calculation method to perform both static and dynamic reserve estimations for the No. 2-1 coal seam at the mine scale and for Working Face 4103. Figure 10 presents the three-dimensional visualization of the No. 2-1 coal seam in the mining area. The model contains 314,080 voxels, with a unit voxel volume of 400 m^3 and an apparent density of 1.39 t/m^3. The calculated coal reserve amounts to 17,462.848 $\times$ 10^4 t.

Figures 11 and 12 present the coal seam models of Working Face 4103 for the years 2022 and 2023, respectively. The models adopt a voxel resolution of 2 m $\times$ 2 m $\times$ 2 m, with 2022 and 2023 selected as the temporal intervals for comparison. The 2022 model of Working Face 4103 was constrained jointly by the mine-scale No. 2-1 coal seam model and the gas drainage boreholes drilled before 2022 within the working face. This model contains 96,568 voxels. With an apparent density of 1.39 t/m^3, the calculated coal reserve is 107.38 $\times 10^4$ t. The 2023 model was similarly constrained by the mine-scale No. 2-1 coal seam model and the gas drainage boreholes drilled before 2023 within the working face. The voxel count increased to 128,712. Using the same apparent density of 1.39 t/m^3, the calculated coal reserve is 143.13 $\times$ 10^4 t. As borehole data are continuously supplemented,

the coal seam model is progressively corrected and updated, enabling dynamic estimation of coal seam resource reserves for the working face.

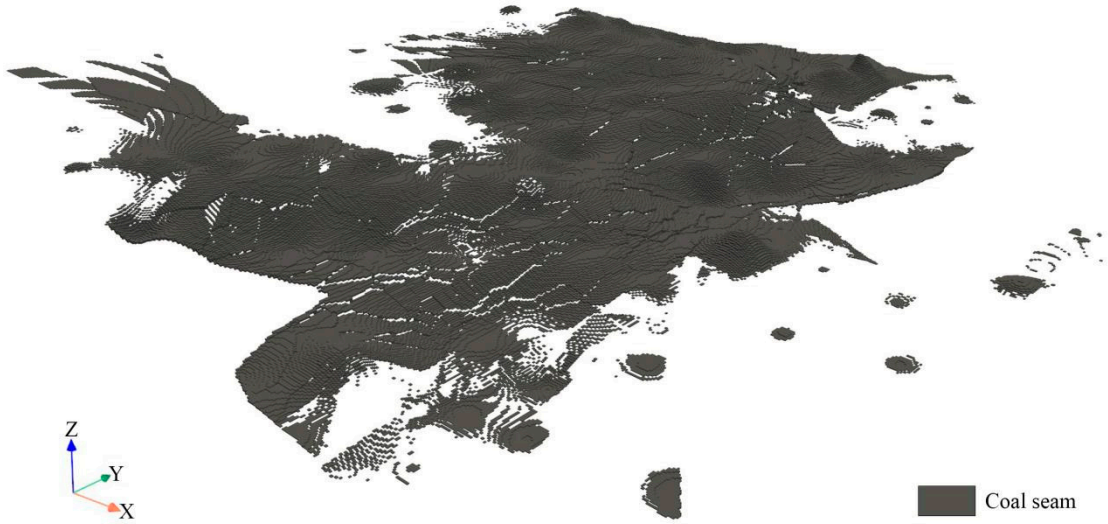


Figure 10. Three-dimensional visualization of the No. 2-1 coal seam at the mine scale.

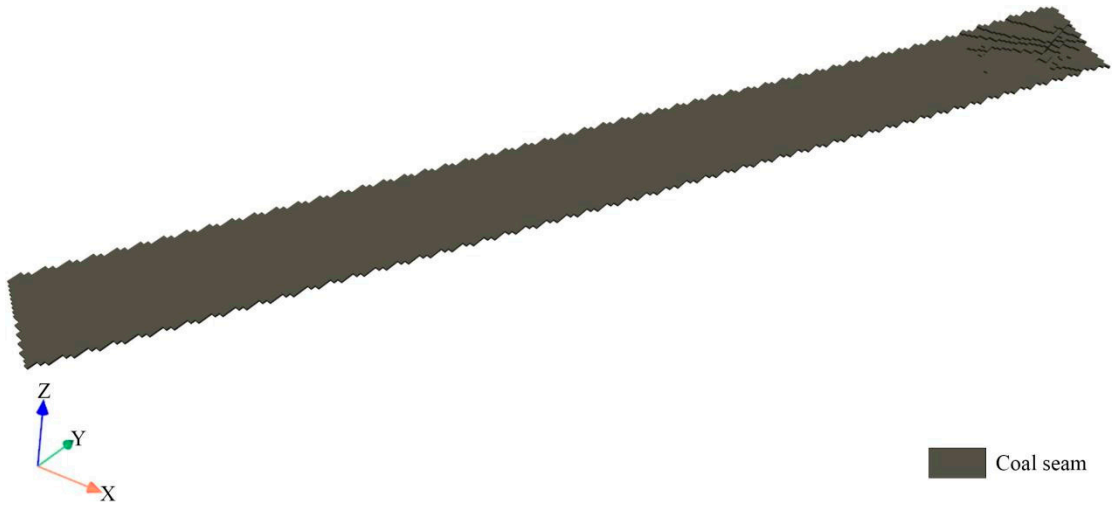


Figure 11. Three-dimensional visualization of the coal seam model of Working Face 4103 in 2022.

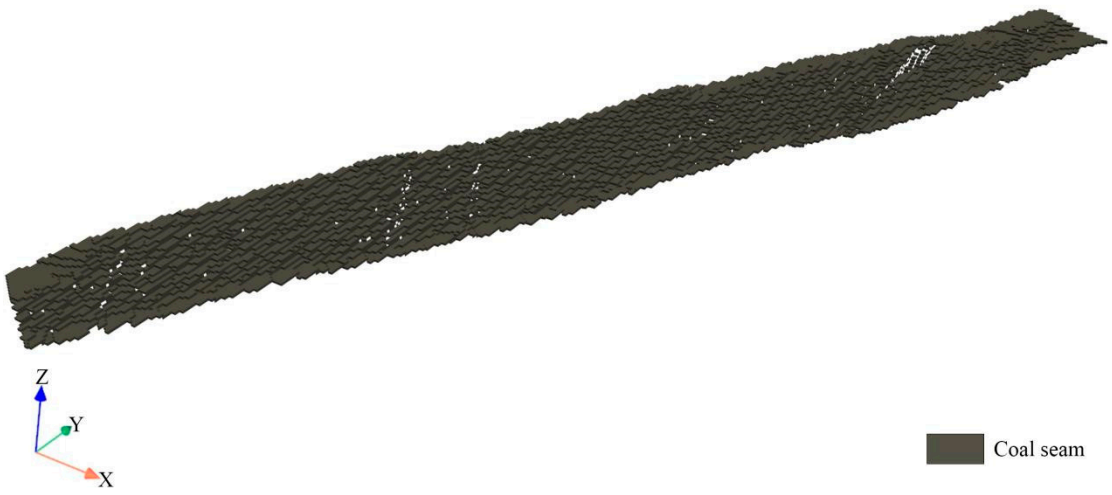


Figure 12. Three-dimensional visualization of the coal seam model of Working Face 4103 in 2023.

4.3. Quantitative Validation, Sensitivity, and Uncertainty Assessment

To further evaluate the performance and applicability of the proposed voxel-based structure–property coupled modeling method, a compact set of validation, sensitivity, and uncertainty tests was conducted. These tests were designed to address three issues: independent assessment of gas content and coal seam geometry estimation, the sensitivity of reserve and attribute results to key modeling parameters, and the uncertainty ranges of reserve estimates under representative scenarios. The purpose of these tests is not to demonstrate a fully general predictive modeling method, but to provide quantitative evidence for the case study implementation under the available data conditions.

For all validation tests, residuals were defined as $e_i = \hat{y}_i - y_i$, where $\hat{y}_i$ and y_i are the predicted and observed values. The metrics were calculated as $ME = n^{-1}\sum e_i$, $MAE = n^{-1}\sum|e_i|$, and $RMSE = \sqrt{n^{-1}\sum e_i^2}$. ME characterizes overall signed bias, whereas MAE and RMSE characterize error magnitude.

Table 6 presents the quantitative validation results. Gas content estimation was assessed by leave-one-out cross-validation using all 555 measurements. In each iteration, one measurement was withheld for validation, and the remaining 554 measurements were used to estimate the gas content at the withheld location. The resulting ME, MAE, and RMSE were -0.0092 m^3/t, 0.4144 m^3/t, and 0.5875 m^3/t, respectively. An ME close to zero indicates no evident systematic overestimation or underestimation under the available data conditions. The working-face coal-seam geometry was evaluated through 30 repeated random holdout splits of the 3468 control points. In each split, 2774 points (approximately 80%) were used for model construction, and the remaining 694 points (approximately 20%) were withheld for validation. The pseudorandom number generator was initialized once with the fixed seed 20260629 before generating the 30 partitions and was not reset between repetitions. For each split, the ME, MAE, and RMSE were calculated separately for roof elevation, floor elevation, and coal thickness using the 694 withheld points; the values reported in Table 6 are the arithmetic means of the corresponding metrics across the 30 repetitions. The resulting mean MAE values were 1.1550 m for roof elevation, 0.9962 m for floor elevation, and 0.6362 m for coal thickness.

Table 6. Validation results for gas content and working-face coal-seam geometry estimation.

Validation Object	Assessment Type	Total *n*	ME	MAE	RMSE
Gas content	LOOCV	555	-0.0092 m^3/t	0.4144 m^3/t	0.5875 m^3/t
Roof elevation	Random holdout	3468	0.0542 m	1.1550 m	1.5657 m
Floor elevation	Random holdout	3468	-0.0077 m	0.9962 m	1.3379 m
Coal thickness	Random holdout	3468	0.0619 m	0.6362 m	1.0701 m

Sensitivity tests were then conducted for voxel resolution and gas content interpolation parameters. The quantitative results are summarized in Table 7.

Table 7. Summary of voxel resolution and gas content interpolation parameter sensitivity.

Tested Factor	Model Component	Base Setting	Tested Setting	Sensitivity Result
Voxel resolution	Mine-scale reserve	10 × 10 × 4 m	8 × 8 × 4 m, 10 × 10 × 4 m, 15 × 15 × 6 m, 20 × 20 × 8 m	−0.72% to +0.32%
Voxel resolution	Working face reserve	2 × 2 × 2 m	1 × 1 × 1 m, 2 × 2 × 2 m, 4 × 4 × 2 m, 4 × 4 × 4 m	−0.6669% to +0.5373%
IDW power	Gas content distribution	Power = 2 Neighbors = 15	Power = 1, 2, 3; Neighbors = 15	std 0.1577 to 0.1867 m^3/t;
Neighbor number	Gas content distribution	Power = 2 Neighbors = 15	Power = 2; Neighbors = 10, 15, 20	std 0.1601 to 0.1842 m^3/t

The base IDW setting for gas content estimation was power = 2 with 15 neighboring samples. In the power sensitivity test, power was varied from 1 to 3, while the neighbor number remained at 15. In the neighbor number test, the number of neighboring samples was varied from 10 to 20, while the power remained at 2. The standard deviation in gas content estimates varied from 0.1577 to 0.1867 m^3/t in the power test and from 0.1601 to 0.1842 m^3/t in the neighbor number test, indicating limited but measurable distributional sensitivity.

Uncertainty was further examined through one-factor voxel resolution tests and paired voxel resolution–density reserve scenarios. According to Equation (8), apparent density directly scales the calculated reserve, whereas voxel resolution affects the discretized representation of coal seam boundaries and the volume of voxels classified as coal.

The reported mine-scale and working face models were retained as the reference models and were not reconstructed when defining the base reserves. For the one-factor voxel resolution tests summarized in Table 7, voxel models were reconstructed from the same original project data, while the geological constraints, model extent, interpretation conditions, interpolation settings, and apparent density of 1.3900 t/m^3 were held constant. For the paired scenarios summarized in Table 8, the geometry of each selected resolution model was retained, and its reserve was recalculated using the corresponding low or high apparent density. The low- and high-density values were obtained by applying ±3% perturbations to the base density, yielding 1.3483 t/m^3 and 1.4317 t/m^3, respectively. The lower and upper estimates in Table 8, therefore, represent predefined paired resolution–density scenarios rather than extrema from a full factorial combination of all tested settings.

Table 8. Reserve estimates under paired voxel resolution and apparent density scenarios.

Scale	Base Reserve/10^4 t	Scenario Range/10^4 t	Relative Variation
Mine scale	17,462.8480	16,991.6016 to 17,857.9046	−2.6986% to +2.2623%
Working face scale	143.1300	139.3561 to 147.0027	−2.6367% to +2.7057%

As shown in Table 8, the mine-scale reference reserve was 17,462.8480 × 10^4 t. Under the paired voxel resolution and apparent density scenarios, the lower and upper reserve estimates were 16,991.6016 × 10^4 t and 17,857.9046 × 10^4 t, corresponding to relative variations of −2.6986% and +2.2623%, respectively. At the working face scale, the reference reserve was 143.1300 × 10^4 t, and the paired scenario reserve estimates ranged from 139.3561 × 10^4 t to 147.0027 × 10^4 t, corresponding to relative variations of −2.6367% and +2.7057%, respectively.

These ranges represent deterministic variations under the selected voxel resolution and apparent-density assumptions. They should not be interpreted as probabilistic confidence intervals or as complete uncertainty propagation through the entire modeling workflow.

5. Discussion

5.1. Extensibility of Structural and Attribute Information Integration in the Coupled Model

To further examine the superposition adaptability of the proposed structure–property coupled modeling method in multi-source information integration, key geological elements, such as faults and protective coal pillars, were selected and systematically integrated with the previously constructed coal seam–gas coupled model. The core technical pathway of this validation is to use voxels as unified information carrier units, progressively superimposing multi-source heterogeneous geological spatial information and attribute parameters

layer by layer, thereby achieving an integrated multi-dimensional representation of geological information.

In the implementation process, the integration of key geological elements (e.g., faults and protective coal pillars) followed a collaborative model superposition strategy. Within the target study area, voxel sub-models were constructed based on the newly introduced geological data, ensuring consistency in the spatial coordinate system and resolution with the original coal seam–gas coupled model. Subsequently, a coupling mapping algorithm was automatically invoked to match each voxel in the new sub-model with its corresponding voxel in the original coupled model, assigning additional geological structural features or attribute parameters accordingly. In this way, seamless integration of newly introduced structural and attribute information into the original coupled model was achieved, ensuring spatial consistency and attribute coherence after integration.

In Figure 13, the red rectangular frame shows a magnified view of a selected voxel. The red point within the frame represents the selected voxel location, and its associated information can be displayed in a dialog box. It can be observed that, based on the integrated coal seam–gas coupled model, additional information such as faults, reserve blocks, and protective coal pillars has been incorporated, forming a comprehensive model characterized by layer-by-layer superposition of structural and attribute information. The results indicate that the model has good scalability and superposability in coupling multi-level and multi-type information. Moreover, as illustrated in Figure 13, the structural and attribute information of any voxel at any spatial location can be readily retrieved.

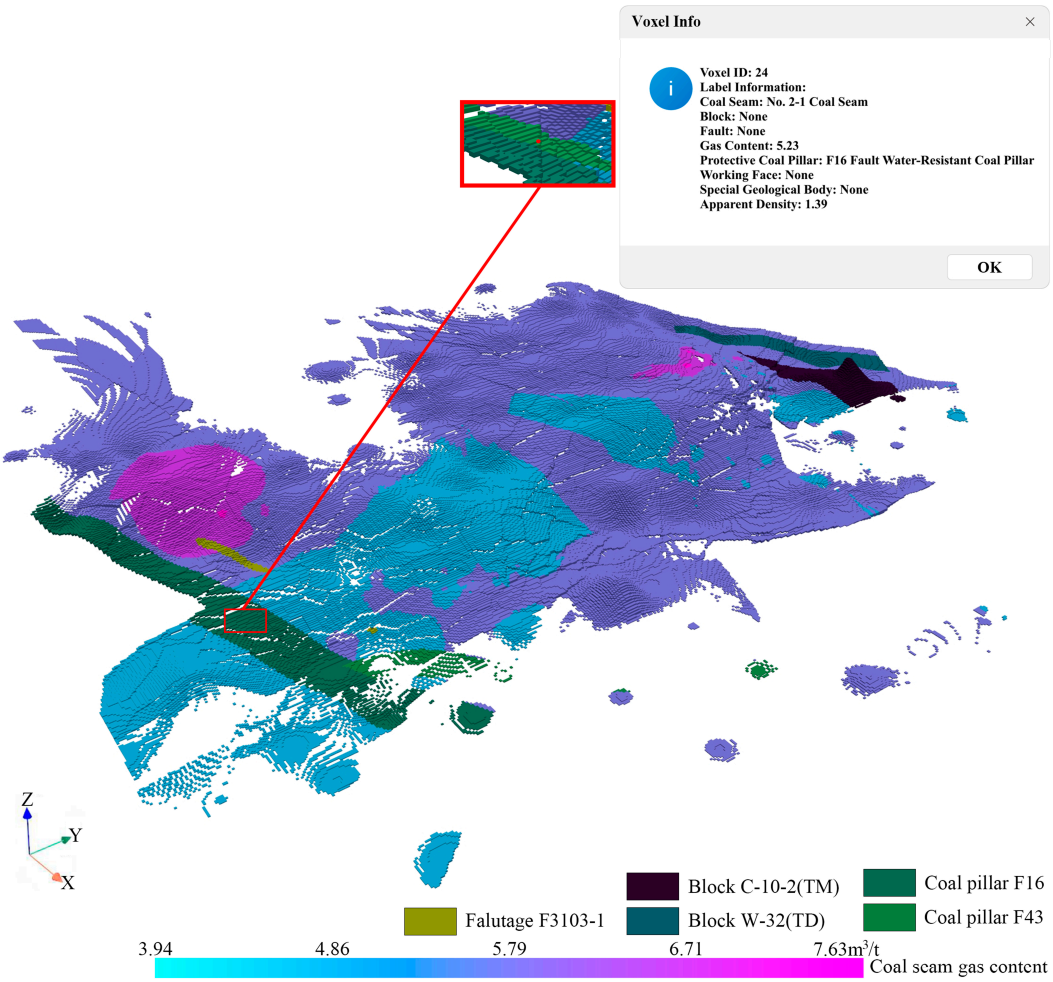


Figure 13. Results of multi-structure–property coupled superposition.

5.2. Engineering Consistency of Reserve Estimation

To evaluate the engineering consistency of the proposed structure–property coupled voxel model in resource reserve estimation, production data from the Hemei No. 3 Coal Mine were used to compare the estimation results derived from the coupled model with those obtained using the traditional geological block method or engineering estimation at both the mine scale and the working-face scale. This comparison was conducted to examine the engineering consistency of the voxel-based reserve estimation results, as well as the variation characteristics of the estimation results with additional data input.

(1) Mine-Scale Reserve Estimation Consistency

According to the mine production geological report, the reserves of the No. 2-1 coal seam are 17,176 $\times$ 10^4 t, while the resource reserves estimated using the proposed coupled modeling method are 17,462.848 $\times$ 10^4 t, corresponding to a relative difference of 1.67%. This result suggests that the reserve estimation derived from the voxel-based coupled model is in good agreement with that obtained using the traditional geological block method, indicating that the voxel-based reserve estimate is consistent with the traditional geological block estimate under the current data conditions of the study area.

(2) Working-Face-Scale Reserve Estimation Consistency

Taking the 4103 working face as an example, its area was determined to be 0.144 km^2 according to the mining engineering plan and related geological data. Reserve estimation was then carried out using the initial voxel model constructed from gas drainage borehole data collected before 2022 and the optimized voxel model updated in 2023 after data supplementation. The results show that the estimated reserve of the 2022 model was 107.38 $\times$ 10^4 t, with a relative difference of 31%, whereas the estimated reserve of the updated 2023 model, which incorporated supplementary mining dynamic monitoring data and refined geological interpretation results, was 143.13 $\times$ 10^4 t, and the relative difference decreased to 8.4%. This change indicates that, with the continuous addition of constraint data such as borehole data, the coupled model becomes more consistent with the engineering reference estimate and better reflects the updated geological constraints of the working face. This suggests that the proposed method can support dynamic reserve updating at the working-face scale under the current data conditions.

A comprehensive analysis of the results at both the mine scale and the working-face scale shows that the proposed method can be used to estimate coal seam reserves based on a unified structure–property coupled model, while also reflecting changes in reserve estimates after geological data supplementation. These comparisons should be interpreted as engineering consistency assessments rather than as independent predictive validation, because both the voxel-based estimates and the reference estimates depend on geological interpretation, data density, coal seam thickness estimation, and density assumptions.

5.3. Applicability Scope of the Proposed Method

Although the structure–property coupling modeling method proposed in this study enables the integrated representation of geological structural information and attribute information within a unified voxel space, and supports model updating and resource reserve analysis, its primary focus is on constructing a unified framework for three-dimensional geological information organization, rather than establishing a complete and universal algorithmic system for structural field reconstruction and attribute field inversion under complex geological conditions. Therefore, the proposed method is more suitable for three-dimensional coal mine modeling and analysis scenarios with a certain degree of geological interpretation and data support, particularly for tasks involving structural representation, attribute coupling, model updating, and resource reserve statistical analysis in an integrated

manner. For cases with more complex structural conditions, weaker data constraints, or more diverse attribute types, the accuracy of structural field and attribute field construction still depends on more advanced structural modeling methods, attribute modeling methods, and supporting constraint information. The application analysis presented in this study is mainly based on data from the Hemei No. 3 Coal Mine and the 4103 working face, with emphasis on coal seam structural representation, gas attribute coupling, and resource reserve estimation. The results indicate that the proposed method shows practical usefulness under the existing data conditions of the study area; however, its applicability still needs to be further validated in more mining areas, across a wider range of attribute types, and under more complex geological conditions. Future research may build on the present framework by incorporating structural modeling in complex tectonic zones, high-precision attribute inversion, independent exposure data, and probabilistic uncertainty propagation.

5.4. Quantitative Sensitivity and Uncertainty Assessment

The additional sensitivity tests show that voxel resolution, interpolation parameters, and density assumptions influence the coupled modeling results to different degrees. With the apparent density fixed at 1.3900 t/m^3, the mine-scale reserve estimate varied from −0.72% to +0.32% among the tested voxel resolutions, whereas the working-face-scale estimate varied from −0.6669% to +0.5373% relative to the internal base case. These results indicate modest resolution sensitivity at both scales, with a slightly broader variation range at the working-face scale.

The IDW parameter tests show that the tested settings influenced the spatial dispersion of gas content estimates. The standard deviation varied within the ranges reported in Table 7 under both the power and neighbor number tests.

The scenario-based assessment further shows that voxel resolution and apparent-density assumptions influence reserve estimation at both modeling scales. Changes in voxel resolution affect the discretized representation of coal seam boundaries and the number or volume of voxels classified as coal, whereas apparent density directly scales the calculated reserve. The resulting ranges provide a first-order indication of reserve variation under the tested assumptions. However, structural interpretation errors, attribute estimation uncertainty, borehole distribution effects, and input data errors were not propagated jointly. The reported ranges should, therefore, be interpreted as case-specific deterministic scenario ranges rather than complete probabilistic uncertainty estimates.

6. Conclusions

This study established and evaluated an application-oriented voxel workflow for coupling geological structure, property information, and reserve calculations. The workflow defines a common voxel domain, reconstructs geological boundary surfaces, assigns a structural label to each voxel, estimates properties only within admissible structural domains, and aggregates coal seam voxels for reserve calculation and sequential updating. Its methodological contribution is this reproducible organization and update procedure within a common voxel index, rather than a new interpolation or general predictive algorithm.

In the Hemei No. 3 Mine case study, leave-one-out validation of 555 gas content measurements yielded ME, MAE, and RMSE values of −0.0092, 0.4144, and 0.5875 m^3/t, respectively. Thirty repeated 80%/20% holdout tests using 3468 geometry control points yielded mean MAEs of 1.1550 m for roof elevation, 0.9962 m for floor elevation, and 0.6362 m for coal thickness. The mine-scale voxel reserve differed from the traditional geological-block estimate by 1.67%. At Working Face 4103, incorporation of additional borehole constraints increased the reserve estimate from 107.38×10^4 t to 143.13×10^4 t and reduced its relative difference from the engineering reference estimate from 31% to

8.4%. With density fixed, voxel resolution changes produced reserve variations of −0.72% to +0.32% at the mine scale and −0.6669% to +0.5373% at the working-face scale. The paired resolution–density scenarios produced deterministic reserve variations of −2.6986% to +2.2623% and −2.6367% to +2.7057%, respectively.

These findings demonstrate case-specific feasibility and quantify performance and sensitivity under the tested data and parameter settings. The block method and engineering reference comparisons are consistency checks, not independent predictive validation, and the reported scenario ranges are deterministic rather than probabilistic confidence intervals. The evidence is limited to one mine; independent roadway exposure or production data were not available, and structural, attribute, density, borehole distribution, and input data uncertainties were not propagated jointly. Future work should test the workflow in additional mines, use independent exposure or production data, and perform probabilistic uncertainty propagation. Within these limits, the workflow provides a practical basis for consistent geological information organization, spatial query, and repeatable reserve updating.

Author Contributions: Conceptualization, Y.Z. and G.W.; methodology, Y.Z. and Y.F.; software, Y.Z. and X.Z.; validation, Y.Z., H.X. and X.Z.; formal analysis, Y.Z. and Y.F.; investigation, Y.Z. and H.X.; resources, G.W.; data curation, Y.Z., H.X. and X.Z.; writing—original draft preparation, Y.Z.; writing—review and editing, G.W., Y.F. and X.Z.; visualization, Y.Z.; supervision, G.W.; project administration, G.W.; funding acquisition, G.W. All authors have read and agreed to the published version of the manuscript.

Funding: This work was funded by the National Science and Technology Major Project of China (2024ZD1001802-2-2), the National Natural Science Foundation of China (U25A20783), and a horizontal research project commissioned by Shaanxi Coalfield Geological Exploration Research Institute Co., Ltd. (Project No. SMDZ-HW-2026-060).

Data Availability Statement: The data presented in this study are available upon request from the corresponding author. The data are not publicly available due to confidentiality agreements and commercial restrictions associated with the mining production data.

Acknowledgments: The authors gratefully acknowledge Hemei No. 3 Mine for providing the geological and production data used in this study. The authors also acknowledge the institutional and technical support provided by the School of Resources and Environment and the Henan Key Laboratory of Coal Measure Unconventional Resources Accumulation and Exploitation, Henan Polytechnic University. In addition, the authors appreciate the academic and methodological discussions contributed by the College of Geoexploration Science and Technology, Jilin University.

Conflicts of Interest: Author Xiao Zhou is employed by the company Shaanxi Provincial Coalfield Geology Group Co., Ltd. The remaining authors declare that the research was conducted in the absence of any commercial or financial relationships that could be construed as a potential conflict of interest.

References

1. Wang, G.; Ren, H.; Zhao, G.; Zhang, D.; Wen, Z.; Meng, L.; Gong, S. Research and practice of intelligent coal mine technology systems in China. *Int. J. Coal Sci. Technol.* **2022**, *9*, 24. [CrossRef]
2. Mao, S. Development of coal geological information technologies in China. *Int. J. Coal Sci. Technol.* **2020**, *7*, 320–328. [CrossRef]
3. Cao, X.; Liu, Z.; Hu, C.; Song, X.; Quaye, J.A.; Lu, N. Three-Dimensional Geological Modelling in Earth Science Research: An In-Depth Review and Perspective Analysis. *Minerals* **2024**, *14*, 686. [CrossRef]
4. Wen, G.C.; Wang, Y.B.; Feng, Y.J.; Zhou, Y.B.; Zhang, Y.F.; Zhao, M.Y. Exploration on the construction of a transparent 3D geological environment in underground coal mine. *J. Henan Polytech. Univ.* **2025**, *44*, 71–80. (In Chinese) [CrossRef]
5. Nobahar, P.; Xu, C.; Dowd, P.; Shirani Faradonbeh, R. Exploring Digital Twin Systems in Mining Operations: A Review. *Green Smart Min. Eng.* **2024**, *1*, 474–492. [CrossRef]

6. Don, M.G.; Wanasinghe, T.R.; Gosine, R.G.; Warrian, P.J. Digital Twins and Enabling Technology Applications in Mining: Research Trends, Opportunities, and Challenges. *IEEE Access* **2025**, *13*, 6945–6963. [CrossRef]
7. Li, D.; Peng, S.; Guo, Y.; Lin, P. Development status and prospect of geological guarantee technology for intelligent coal mining in China. *Green Smart Min. Eng.* **2024**, *1*, 433–446. [CrossRef]
8. Calcagno, P.; Chilès, J.P.; Courrioux, G.; Guillen, A. Geological modelling from field data and geological knowledge: Part I. Modelling method coupling 3D potential-field interpolation and geological rules. *Phys. Earth Planet. Inter.* **2008**, *171*, 147–157. [CrossRef]
9. Caumon, G.; Collon-Drouaillet, P.; Le Carlier de Veslud, C.; Viseur, S.; Sausse, J. Surface-Based 3D Modeling of Geological Structures. *Math. Geosci.* **2009**, *41*, 927–945. [CrossRef]
10. Grose, L.; Aillères, L.; Laurent, G.; Jessell, M. LoopStructural 1.0: Time-aware geological modelling. *Geosci. Model Dev.* **2021**, *14*, 3915–3937. [CrossRef]
11. Kang, H.; Wang, B.; Gao, F.; Zhang, Y.; Fan, Z.; Li, S.; Xu, X.; Chen, P. Current status and prospects of coal mining science and technology in China. *GeoEnergy Commun.* **2025**, *1*, 3. [CrossRef]
12. Li, J.; Liu, P.; Wang, K.; Zhang, W.; Wang, Y.; Xu, Y. 3D geological implicit modeling method of regular voxel splitting based on hierarchical interpolation data. *Sci. Rep.* **2022**, *12*, 13840. [CrossRef] [PubMed]
13. Jiang, Z.Y.; Xie, H.B.; Wen, G.C.; Huang, X.R. Design and application of electromagnetic radio MWD system of drilling trajectory measurement in underground coal mine. *Coal Geol. Explor.* **2017**, *45*, 156–161. (In Chinese) [CrossRef]
14. Kessler, H.; Mathers, S.; Sobisch, H.G. The capture and dissemination of integrated 3D geospatial knowledge at the British Geological Survey using GSI3D software and methodology. *Comput. Geosci.* **2009**, *35*, 1311–1321. [CrossRef]
15. Turner, A.K. Challenges and trends for geological modelling and visualisation. *Bull. Eng. Geol. Environ.* **2006**, *65*, 109–127. [CrossRef]
16. De la Varga, M.; Schaaf, A.; Wellmann, F. GemPy 1.0: Open-source stochastic geological modeling and inversion. *Geosci. Model Dev.* **2019**, *12*, 1–32. [CrossRef]
17. Feng, Y.J.; Wen, G.C.; Wu, B.J.; Hu, Z.D. A method for identifying faults within mining faces based on spatial statistics. *Coal Geol. Explor.* **2023**, *51*, 19–26. (In Chinese) [CrossRef]
18. Lark, R.M.; Mathers, S.J.; Thorpe, S.; Arkley, S.L.B.; Morgan, D.J.; Lawrence, D.J.D. A statistical assessment of the uncertainty in a 3-D geological framework model. *Proc. Geol. Assoc.* **2013**, *124*, 946–958. [CrossRef]
19. Wellmann, F.; Caumon, G. 3-D structural geological models: Concepts, methods, and uncertainties. *Adv. Geophys.* **2018**, *59*, 1–121. [CrossRef]
20. Jessell, M.W.; Aillères, L.; Kemp, E.A. Towards an integrated inversion of geoscientific data: What price of geology? *Tectonophysics* **2010**, *490*, 294–306. [CrossRef]
21. Zhou, C.; Du, Z.; Ouyang, J.; Zhang, Z.; Liu, Z. A 3D geological model and cutting algorithm based on a vertically projected triangulated network. *Comput. Geosci.* **2020**, *143*, 104562. [CrossRef]
22. Zehner, B.; Börner, J.H.; Görz, I.; Spitzer, K. Workflows for generating tetrahedral meshes for finite element simulations on complex geological structures. *Comput. Geosci.* **2015**, *79*, 105–117. [CrossRef]
23. Pellerin, J.; Botella, A.; Bonneau, F.; Mazuyer, A.; Chauvin, B.; Lévy, B.; Caumon, G. RINGMesh: A programming library for developing mesh-based geomodeling applications. *Comput. Geosci.* **2017**, *104*, 93–100. [CrossRef]
24. Pakyuz-Charrier, E.; Lindsay, M.; Ogarko, V.; Giraud, J.; Jessell, M. Monte Carlo simulation for uncertainty estimation on structural data in implicit 3-D geological modeling, a guide for disturbance distribution selection and parameterization. *Solid Earth* **2018**, *9*, 385–402. [CrossRef]
25. Wu, Q.; Xu, H.; Zou, X. An effective method for 3D geological modeling with multi-source data integration. *Comput. Geosci.* **2005**, *31*, 35–43. [CrossRef]
26. Jessell, M.; Guo, J.; Li, Y.; Lindsay, M.; Scalzo, R.; Giraud, J.; Pirot, G.; Cripps, E.; Ogarko, V. Into the Noddyverse: A massive data store of 3D geological models for machine learning and inversion applications. *Earth Syst. Sci. Data* **2022**, *14*, 381–392. [CrossRef]
27. Lark, R.M.; Thorpe, S.; Kessler, H.; Mathers, S.J. Interpretative modelling of a geological cross section from boreholes: Sources of uncertainty and their quantification. *Solid Earth* **2014**, *5*, 1189–1205. [CrossRef]
28. Kim, H.S.; Ji, Y. Three-dimensional geotechnical-layer mapping in Seoul using borehole database and deep neural network-based model. *Eng. Geol.* **2022**, *297*, 106489. [CrossRef]
29. Ma, Z.Y.; Zhang, S.; Li, J.; Qiao, Y.K.; Sun, H.F.; Bouchaala, F. A new integrated 3D modeling method based on multisource heterogeneous geological data and its application. *China Geol.* **2026**, *9*, 383–399. [CrossRef]
30. Wellmann, J.F.; De La Varga, M.; Murdie, R.E.; Gessner, K.; Jessell, M. Uncertainty estimation for a geological model of the Sandstone greenstone belt, Western Australia—Insights from integrated geological and geophysical inversion in a Bayesian inference framework. *Geol. Soc. Lond. Spec. Publ.* **2018**, *453*, 41–56. [CrossRef]
31. Liu, L.; Li, T.; Ma, C. Research on 3D Geological Modeling Method Based on Deep Neural Networks for Drilling Data. *Appl. Sci.* **2024**, *14*, 423. [CrossRef]

32. De Pasquale, G.; Linde, N.; Doetsch, J.; Holbrook, W.S. Probabilistic inference of subsurface heterogeneity and interface geometry using geophysical data. *Geophys. J. Int.* **2019**, *217*, 816–831. [CrossRef]
33. Schorpp, L.; Straubhaar, J.; Renard, P. Automated Hierarchical 3D Modeling of Quaternary Aquifers: The ArchPy Approach. *Front. Earth Sci.* **2022**, *10*, 884075. [CrossRef]
34. Gong, W.; Juang, C.H.; Martin, J.R.; Tang, H.; Wang, Q.; Huang, H. Coupled characterization of stratigraphic and geo-properties uncertainties—A conditional random field approach. *Eng. Geol.* **2021**, *294*, 106348. [CrossRef]
35. Li, X.Y.; Zhang, L.M.; Li, J.H. Using conditioned random field to characterize the variability of geologic profiles. *J. Geotech. Geoenviron. Eng.* **2016**, *142*, 04015096. [CrossRef]
36. Qi, X.H.; Li, D.Q.; Phoon, K.K.; Cao, Z.J.; Tang, X.S. Simulation of geologic uncertainty using coupled Markov chain. *Eng. Geol.* **2016**, *207*, 129–140. [CrossRef]
37. Li, J.; Cai, Y.; Li, X.; Zhang, L. Simulating realistic geological stratigraphy using direction-dependent coupled Markov chain model. *Comput. Geotech.* **2019**, *115*, 103147. [CrossRef]
38. Ouyang, J.; Zhou, C.; Liu, Z.; Zhang, G. Triangulated irregular network-based probabilistic 3D geological modelling using Markov chain and Monte Carlo simulation. *Eng. Geol.* **2023**, *320*, 107131. [CrossRef]
39. Laloy, E.; Hérault, R.; Jacques, D.; Linde, N. Training-image based geostatistical inversion using a spatial generative adversarial neural network. *Water Resour. Res.* **2018**, *54*, 381–406. [CrossRef]
40. Høyer, A.S.; Klint, K.E.S.; Fiandaca, G.; Maurya, P.K.; Christiansen, A.V.; Balbarini, N.; Bjerg, P.L.; Hansen, T.B.; Møller, I. Development of a high-resolution 3D geological model for landfill leachate risk assessment. *Eng. Geol.* **2019**, *249*, 45–59. [CrossRef]
41. Bouayach, N.; Kassou, F.; Rguig, M. 3D combined stratigraphy and geo-properties modeling using probabilistic machine learning. *Eng. Geol.* **2025**, *357*, 108387. [CrossRef]
42. Yang, Z.; Chen, Q.; Cui, Z.; Liu, G.; Dong, S.; Tian, Y. Automatic reconstruction method of 3D geological models based on deep convolutional generative adversarial networks. *Comput. Geosci.* **2022**, *26*, 1135–1150. [CrossRef]

Disclaimer/Publisher's Note: The statements, opinions and data contained in all publications are solely those of the individual author(s) and contributor(s) and not of MDPI and/or the editor(s). MDPI and/or the editor(s) disclaim responsibility for any injury to people or property resulting from any ideas, methods, instructions or products referred to in the content.